Nanoscale

MINIREVIEW

View Article Online
View Journal | View Issue

Cite this: *Nanoscale*, 2016, **8**, 6249

Revealing the ultrafast charge carrier dynamics in organo metal halide perovskite solar cell materials using time resolved THz spectroscopy

C. S. Ponseca Jr.* and V. Sundström

Ultrafast charge carrier dynamics in organo metal halide perovskite has been probed using time resolved terahertz (THz) spectroscopy (TRTS). Current literature on its early time characteristics is unanimous: sub-ps charge carrier generation, highly mobile charges and very slow recombination rationalizing the exceptionally high power conversion efficiency for a solution processed solar cell material. Electron injection from $MAPbI_3$ to nanoparticles (NP) of TiO_2 is found to be sub-ps while Al_2O_3 NPs do not alter charge dynamics. Charge transfer to organic electrodes, Spiro-OMeTAD and PCBM, is sub-ps and few hundreds of ps respectively, which is influenced by the alignment of energy bands. It is surmised that minimizing defects/trap states is key in optimizing charge carrier extraction from these materials.

Received 29th October 2015,
Accepted 7th January 2016

DOI: 10.1039/c5nr08622a

www.rsc.org/nanoscale

1. Introduction

The seemingly unstoppable rise of organo-metal halide perovskite-based (OMHP) solar cells is now becoming a direct competitor to the current leading technology silicon. This has been triggered by the unprecedented increase in its overall power conversion efficiency (PCE) reaching 20.1% in just a few years.[1]

Division of Chemical Physics, Lund University, Getingevagen 60, Lund, Sweden. E-mail: carlito.ponseca@chemphys.lu.se

This dramatic development is a result of the joint efforts of many groups from different fields of solar cell research, *i.e.* organic, dye-sensitized, quantum-dot sensitized and inorganic, which are now focusing on this material. One can anticipate that with this enormous attention, exciting new results will snowball in the coming years. Already, recent reports on this material could probably offer a hint of this scenario: it has been shown that it can be used as light emitting diodes having a bright visible and infrared electroluminescence, was able to demonstrate low lasing thresholds with high quality factors[2] and has been used for water photolysis with an impressive

C. S. Ponseca Jr.

Carl started his research on THz spectroscopy during his Ph.D. studies in the Graduate University for Advanced Studies, Kanagawa, Japan focusing on design and characterization of THz waveguides. He then moved to Kobe University as postdoctoral fellow where he used THz radiation for vibrational spectroscopy of biomolecules, e.g. *amino acids and polypeptides. From 2010, he has been studying charge carrier dynamics in solar cell materials using time-resolved THz spectroscopy. His work in Lund University includes understanding the ultrafast processes in organic, inorganic, dye- and quantum dot-sensitized, and perovskite-based solar cells.*

V. Sundström

Villy Sundström has more than 35 years of experience in photochemistry, ultrafast spectroscopy, molecular structural dynamics, photosynthesis, and solar energy research. Early studies of chemical reaction dynamics and energy and electron transfer in photosynthesis more recently lead to work on novel materials for solar energy conversion, dye-sensitized solar cells, polymer solar cells and now very recently organo-metal-halide perovskite solar cells. Photocatalytic processes underlying production of solar fuels are studied using ultrafast X-ray methods. Time resolved THz spectroscopy is extensively implemented for the study of carrier dynamics in nanostructured solar cell materials.

12.3% solar-to-hydrogen efficiency[3] among others. However, a large part of the OMHP community is dedicated to the optimization of growth, encapsulation, stability, and material development in an effort to realize the highest PCE possible. Due to this, fundamental studies have been taken to the back seat, but if more actively pursued could have offered a better understanding of the behaviour of this material. Consequently, comprehension of the fundamental photophysics of the charge carrier dynamics has remained limited. Among unresolved issues are the nature of the initial photogenerated species, timescale of formation of charges, mobility, scattering time of carriers, and its recombination dynamics. In this minireview we will discuss available results on the early time dynamics, that is, from sub-ps to 1 ns, of charged species in the hope of addressing the above questions. Time resolved terahertz (THz) spectroscopy (TRTS) is primarily used to directly access the photo conductivity of the material providing insight into the nature of charge carriers, their mobility and its time dependence. We also refer to other optical techniques, *e.g.* transient absorption and photoluminescence to complement the TRTS results. We will start our discussion by introducing our and other groups' results on the charge dynamics of neat thin films of $MAPbI_3$ and $MAPbI_{3-x}Cl_x$ in order to elucidate intrinsic properties. Next, we will compare the dynamics of neat OMHP and the perovskite attached to either metal oxide TiO_2 or Al_2O_3, which are used as electron accepting material or as scaffold, respectively. Recent results on femtosecond charge generation dynamics in a single crystal $MAPbI_3$ will also be presented. Then, the use of organic transport materials, *i.e.* PCBM and Spiro-OMeTAD, which have been prevalently utilized as possible substitutes to metal oxides will be discussed. Lastly, we attempt to paint a picture of the early time behavior of this material and its implications to the performance of solar cells. The works presented here are collections of papers in the past few years on the understanding of charge carrier dynamics using TRTS as primary measurement tool. Although there are rather few groups that have access to this facility, and therefore papers based on the results of such measurements are not numerous, the conclusions drawn are unanimous: OMHP materials have nearly ideal solar cell characteristics namely, charge generation in the ultrafast timescale, very high and nearly balanced mobility of charge carriers, and very slow recombination, rationalizing its very high overall PCE.

The primary result of TRTS is the change in conductivity ($\Delta\sigma$) of the material following optical excitation as expressed by the equation:

$$\Delta\sigma = \xi \times (\mu_e + \mu_h) = -\frac{\Delta E_{exc}(\omega)}{\Delta E_{gs}(\omega)} \frac{\varepsilon_0 c}{F e_0} \frac{1}{1 - e^{-\alpha L}} \quad (1)$$

where ξ is quantum yield of charge generation, μ_e and μ_h are the electron and hole mobility, respectively, ΔE_{exc} is the THz electric field transmitted through the sample after photo excitation while ΔE_{gs} is the ground state THz electric field, ε_0 is permittivity of vacuum, c is velocity of light, F is the fluence in ph cm^{-2}, e_0 is the elementary charge, α is the absorption coefficient, and L the thickness of the sample. The quantity that is obtained from the above equation has the unit of mobility in $cm^2\ V^{-1}\ s^{-1}$. By definition, $\Delta\sigma$ is a product of two quantities, quantum yield and mobility. At the earliest timescale, ξ is assumed to be 1, while at longer times this represents the change in charge population at a particular time in the material. The assumption of ξ = 1 means that all absorbed photon is converted to mobile charges. Since accurate measurement of ξ is currently not available in the literature, this assumption means that mobility reported here is the lowest estimate of mobility and that it can be an order higher if one assume this as 10%. As we would be discussing towards the later part of this work, by scanning the full THz waveform and fitting it with the Drude model, it is also possible to independently obtain charge generation efficiency (or quantum yield) and mobility. The interplay between the time-dependent change in charge population and mobility defines the shape of the THz photoconductivity kinetics and spectra. On one hand, the rise in the photoconductivity kinetics elucidates generation of charged species and/or increase in mobility of the charges. On the other hand, decay represents decrease of the mobility (maybe due to relaxation) and/or disappearance of charge carriers either by recombination, or injection to a low mobility acceptor material. The THz photoconductivity spectrum is also a very important and informative tool in analysing the mode of transport of charges. The typical signature for confined or restricted transport is a positive real part and a negative imaginary part of the THz conductivity spectra, while for long range, electron gas-like transport, both the real and imaginary parts are positive.[4] The THz photoconductivity spectrum is obtained by fixing the pump–probe delay at some desired time and sweeping the gating delay to record the THz electric field. THz photoconductivity kinetics, on the other hand, is collected by fixing the gating delay at the peak of the THz electric field while scanning the pump–probe delay within a desired time interval.

Shown in Fig. 1 is the schematic of the set-up while the detailed description of the experiment can be found elsewhere.[5] We have previously reported that by using this technique the injection dynamics, mobility and recombination of charges can be directly probed. In fact we reported the early timescale behavior of several solar cell technologies which includes organic,[6–8] dye-[9] and quantum dot-[10] sensitized, inorganic nanowires,[11] and recently perovskite solar cells.[5,12]

2. Charge dynamics in neat OMHP and OMHP on mesoporous metal oxides

Shown in Fig. 2 is the THz photoconductivity kinetics of neat $MAPbI_3$, $MAPbI_3/Al_2O_3$ and $MAPbI_3/TiO_2$. The neat sample provides information on the intrinsic transport properties of the material, while $MAPbI_3$ on nanostructured Al_2O_3 was studied

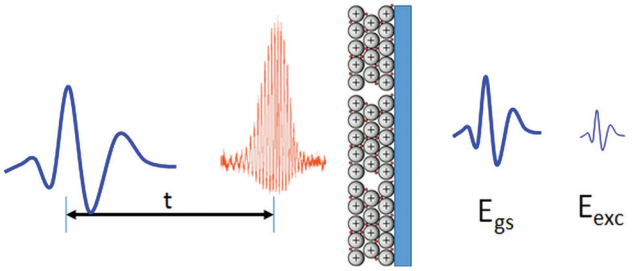

Fig. 1 Schematic diagram of the time resolved THz set-up used in probing charge carrier dynamics in OMHP solar cell. Visible pump pulse (red) is about 80 fs while THz pulse probe is about 1 ps. Transmitted THz electric fields, E_{gs} (ground state) and E_{exc} (excited state), are Fourier transformed and eqn (1) is used to obtain the photoconductivity spectra at desired pump–probe delay ($t_{pump-probe}$) while scanning the gate delay (t_{gate}). For photoconductivity kinetics t_{gate} is fixed at the maximum of THz electric field and $t_{pump-probe}$ is scanned.

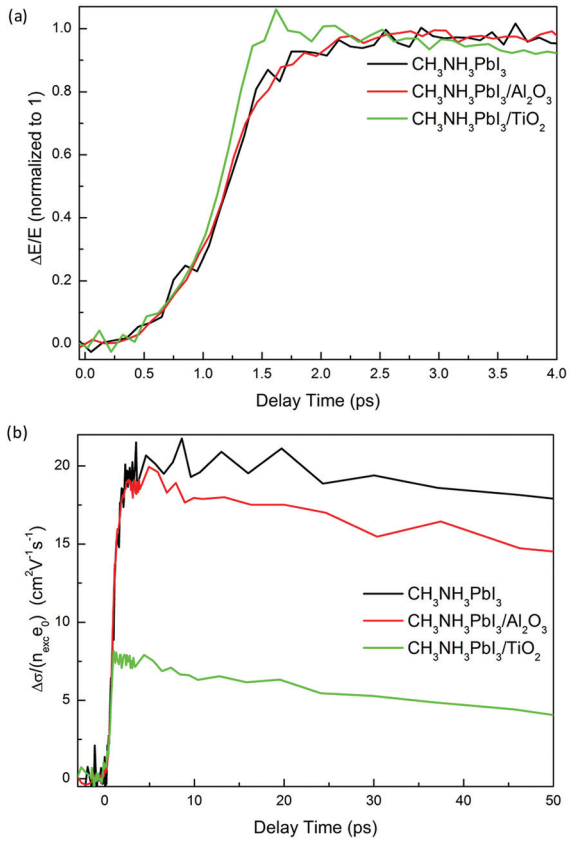

Fig. 2 Early time photoconductivity kinetics of the three samples under study (a) normalized to 1 and (b) normalized to excitation density (λ_{exc} = 400 nm, $I_{exc} = 2 \times 10^{12}$ ph cm^{-2}). Conditions for sample preparation can be found in the ESI of ref. 5. Reprinted with permission from ref. 5. Copyright (2014) American Chemical Society.

to understand the influence of the nanostructure on the charge carrier dynamics. To clarify the role of an electron accepting metal oxide, $MAPbI_3$ is introduced into nanostructured TiO_2. By normalizing the amplitude of the signal to unity, we can compare the rise times of the THz photoconductivity kinetics (Fig. 2a). The initial increase reflects generation of charged species rather than molecular excitons since these types of excitons are tightly bound electron–hole pairs that have no charge. Although it is possible that such excitons are simultaneously generated by the light excitation, it will not influence the conductivity of the sample and therefore cannot be seen by the technique. We also note that since the THz probe energies used here is very low (1 THz = 4 meV), such photoproduct cannot be detected. The rise times of neat $MAPbI_3$ and $MAPbI_3/Al_2O_3$ is characterized by a two-step rise, *i.e.* an instrument limited rise with about 70% of the total signal amplitude, and a 2–3 ps second rise (about 30% of the total amplitude). This can be interpreted in two ways. First, the sub-ps rise is generation of charged species that are loosely bound; they are mobile but not totally free from Coulombic attraction. The second few ps rise can then be assigned to dissociation of these loosely bound electron hole pairs into free charges.[5] Dissociation would result in the increase of mobility and would manifest as additional increase in the THz photoconductivity kinetics, justifying the second step rise. Another possible interpretation is that there is a distribution of exciton and free charge formation. In this scenario, it requires that the binding energy of photoinduced species is heterogeneous. Heterogeneity of binding energy finds it origin from the non-uniformity of sample quality, that is, difference in the concentration of defects. Indeed, recent studies report a range of different binding energies of this material, from a few meV to about 50 meV.[12–17] If this spread in reported values indeed represents a distribution of binding energies, and not just scattered values due to measurement technique issues, then the 70% instantaneous response could correspond to direct formation of free charges, originating from the part of the material with low exciton binding energy, while the 30% few-ps rise would represent delayed dissociation of charged species with higher binding energy. The role of hot exciton and relaxed exciton dissociation can be discounted since a similar two-step rise is also observed from 800 nm pump experiments (manuscript in preparation). It should be stressed that the second step rise could only be observed when a sufficiently low excitation fluence is used ($<2 \times 10^{12}$ ph cm^{-2}). This is because at higher excitation, a higher concentration of charge carriers is created, which would cause charge pair annihilation similar to that observed in organic solar cells.[7] This process would be observed as few-ps fast decay, on a time-scale similar to that of exciton dissociation and the two signals therefore cancelling each other. A similar two-step rise of the THz conductivity is observed for $MAPbI_3/Al_2O_3$. This shows that at least on the early time scale, the charge dynamics of perovskite attached to an inert nanoporous material are similar to that of neat $MAPbI_3$. The film morphology on the other hand exhibits significantly different quality and film coverage.[5] For $MAPbI_3/Al_2O_3$, the film is uniform and the optical density is often larger than 1, while for neat $MAPbI_3$ it is difficult to obtain a uniform film and the optical density is

about 0.5 at the excitation wavelength (400 nm). This could probably be the reason to the better signal to noise ratio in $MAPbI_3/Al_2O_3$ than in neat $MAPbI_3$, while the mobility still is similar for both films (to be discussed below). For $MAPbI_3/TiO_2$, only a one-step ultrafast instrument limited rise was observed. This is reminiscent of our previous reports on ultrafast electron injection from the RuN_3 dye to TiO_2 and from CdSe quantum dots to ZnO, which have similar rise times.[9,10] Therefore, it can be concluded that the injection of electrons from the perovskite to TiO_2 is also sub-ps. Optical transient absorption measurements performed on the same sample at similar experimental conditions show very similar timescale of ultrafast electron injection from $MAPbI_3$ into TiO_2.[5] The favorable energy alignment of the conduction bands of TiO_2 and $MAPbI_3$ breaks any or all remaining strongly bound excitons generated by light excitation in the perovskite on the sub-ps time scale, resulting in just one step ultrafast rise of the THz photoconductivity kinetics.

Normalizing the THz photoconductivity kinetics to the excitation density used (eqn (1)), the mobility obtained per photon absorbed for neat $MAPbI_3$ is 20 $cm^2\ V^{-1}\ s^{-1}$ as shown in Fig. 2(b). Since this is a neat material, the mobility obtained here should be from both electrons and holes. As discussed above there is an ultrafast injection of electrons from perovskite to TiO_2. This means that the 7.5 $cm^2\ V^{-1}\ s^{-1}$ from $MAPbI_3/TiO_2$ should only be coming from the mobility of holes, since the mobility of electrons in TiO_2 is only <0.1 $cm^2\ V^{-1}\ s^{-1}$.[18] Consequently, the electron mobility in neat $MAPbI_3$ must be 12.5 $cm^2\ V^{-1}\ s^{-1}$ since the mobility of hole was estimated to be 7.5 $cm^2\ V^{-1}\ s^{-1}$, yielding a total mobility of 20 $cm^2\ V^{-1}\ s^{-1}$. It should be noted that the mobilities of electrons and holes in $MAPbI_3/Al_2O_3$ are very similar to those in neat $MAPbI_3$ since the overall amplitude of the photoconductivity kinetics is very similar in the two samples, showing that Al_2O_3 scaffold does not alter the mobility. These findings highlight two important properties of the OMHP materials. First, both electron and hole mobility is very high, at least several orders of magnitude higher than carrier mobilities in organic solar cell materials, *e.g.* APFO3:PCBM[6] and TQ1:PCBM,[7] which is 0.005 $cm^2\ V^{-1}\ s^{-1}$ and 0.2 $cm^2\ V^{-1}\ s^{-1}$ respectively. Due to this high mobility, and related long diffusion length, charges will quickly diffuse through the active material to reach the electrodes for efficient extraction. Second, not only that both charges are mobile, both mobilities are quite similar (within a factor of two). This prevents creation of built-in electric fields and space charge-limited photocurrents that lowers the PCE. Despite these interesting properties of OMHP materials, the mobility remains modest in comparison with established silicon solar cell materials, typically having mobilities of 1400 $cm^2\ V^{-1}\ s^{-1}$ and 500 $cm^2\ V^{-1}\ s^{-1}$ for electrons and holes, respectively.[19] However, such a comparison should be put into a proper context. OMHP is a "kitchen chemistry-prepared" polycrystalline material, while silicon solar cells use highly sophisticated industry developed single crystalline grown wafers. Developing preparation methods that can lead to low defect, high quality single crystal perovskite could increase its mobility significantly.

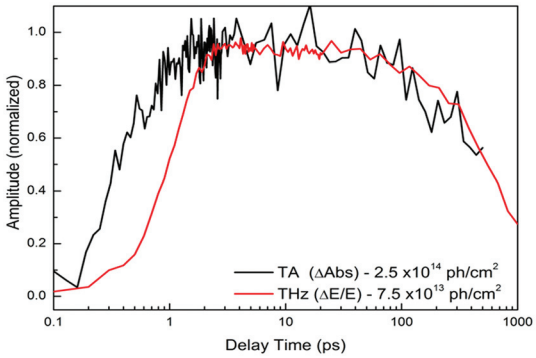

Fig. 3 TA and TRTS kinetics of neat $MAPbI_3$ showing similar decay rate up to 1 ns. Reprinted with permission from ref. 5. Copyright (2014) American Chemical Society.

With the high mobility obtained above, the next question that arises is, how long would the charges be able to sustain this mobility? It is highly favorable for solar cell devices to have charges with high mobility at longer timescales, since extraction to the electrodes would be more efficient. In organic solar cell materials, TQ1:PCBM for example, relaxation of mobility is seen to be in the few hundreds of ps.[7] Comparison of TRTS and TA kinetics is a useful approach to probe relaxation of mobility since THz photoconductivity is a product of charge population and mobility, while TA probes the change of absorbance of a sample which provides direct information on the population dynamics only. Shown in Fig. 3 is the kinetics obtained with the two techniques, measured at similar excitation intensities and for the same neat $MAPbI_3$ sample. The signal to noise of the TA kinetics is rather low due to scattering of the probe light (970 nm) caused by the micrometer-size grains of the sample. Within the experimental error and up to 1 ns, the decay of the kinetics are identical. This means that the decay of the THz photoconductivity kinetics is due to population decay only, since the TA kinetics have very similar decay. Consequently, the mobility of charge carriers remains constant on this timescale, otherwise the decay would be faster than that observed in the TA measurements. In addition, the THz photoconductivity spectra in Fig. 4 also support this interpretation. For neat $MAPbI_3$, the shape of the spectra is very similar from 10 ps (black trace with squares) up to 1 ns, implying that the mobility stays constant within this time window. Interestingly, despite its high mobility and long lifetime, the THz photoconductivity spectra have a positive real part and negative imaginary part, characteristic of a confined mode of charge transport, *i.e.* charges find scattering centers, *e.g.* grain boundaries, traps or defects, at distances shorter than the material's diffusion length.[4,9,10,14] This strongly suggests that the domain size of the sample does not permit long range electron–gas like transport of charge.

The above results have very important implications to solar cell devices. Not only that charges are generated on the ultrafast timescale and mobility is very high, it remains high for at least 1 ns. Recombination, geminate or otherwise, is not preva-

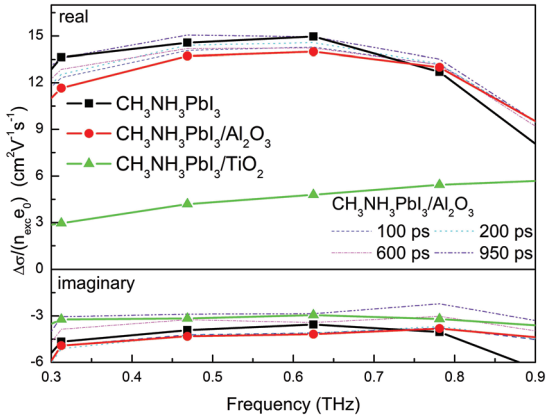

Fig. 4 THz photoconductivity spectra of the three samples. Reprinted with permission from ref. 5. Copyright (2014) American Chemical Society.

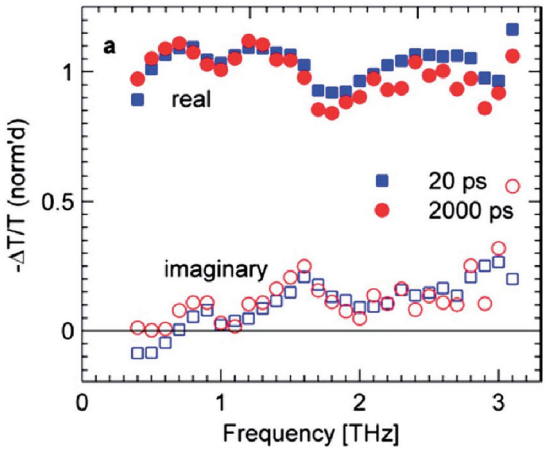

Fig. 5 Normalized, complex THz photoinduced absorption spectra of vapour-deposited $CH_3NH_3PbI_{3-x}Cl_3$ (closed symbols – real parts, open symbols – imaginary parts). Reprinted with permission from ref. 21. Copyright (2014) Royal Society of Chemistry.

lent up to at least 1 ns giving the charges the opportunity to be extracted at the electrodes. Measurements with the related time resolved microwave conductivity technique, in fact show that high mobility extends out to the microsecond time scale.[5] A simple one dimensional diffusion calculation using a mobility of 12.5 $cm^2\ V^{-1}\ s^{-1}$ (for electrons) and a thickness of 200 nm (typical for solar cell devices) results in a diffusion time of hundreds of ps only to transverse the film thickness. This illustrates that most, if not all, photogenerated charges are removed from the active material, rationalizing the very high power conversion efficiency. Despite this, the domain size should be increased if one desires longer diffusion lengths.

Wehrenfennig *et al.* measured charge carrier mobility in thin films of $MAPbI_3$ and $MAPbI_{3-x}Cl_x$ by using time resolved THz spectroscopy as well.[20] They found that the lower bound for the mobility is 11.6 $cm^2\ V^{-1}\ s^{-1}$ for $MAPbI_{3-x}Cl_x$ and 8 $cm^2\ V^{-1}\ s^{-1}$ for $MAPbI_3$, which is of the same order of magnitude as the above results. Differences in the exact value of the mobility can be related to slight differences in sample characteristics, *i.e.* defects, traps, *etc.*, brought about by somewhat different preparation methods. Generation of charges was concluded to be instrument limited,[20] *i.e.* sub-ps, since a sharp rise in the THz photoconductivity kinetics was observed. From excitation intensity dependence of the decay of TRTS kinetics, Wehrenfennig *et al.*[20] were able to extract the Langevin rate for recombination. It was shown that the second order recombination rate defies the Langevin limit by at least four orders of magnitude, *i.e.* 8.7×10^{-11} *versus* 4.2×10^{-6} $cm^3\ s^{-1}$ for $MAPbI_{3-x}Cl_x$. Similar differences in the recombination rates were observed for $MAPbI_3$ (1 : 1) and $MAPbI_3$ (3 : 1), where the ratio is between the amount Pb and I_3 in the sample. From the obtained high mobility and very slow recombination rate, a diffusion length of at least 1 μm was estimated.[20] Such very slow recombination rate as well as micrometer long diffusion length were also confirmed by Savenije *et al.*[12] This unique characteristics is suggested to be emanating from the preferential localization of electrons and holes in different regions within the perovskite unit cell, which could result in reduction of spatial overlap of the wave functions, thereby lowering their probability to meet and recombine". In a follow-up paper of the same group, Wehrenfennig and co-workers measured the mobility of vapour-deposited films of $MAPbI_{3-x}Cl_x$.[21] The obtained overall mobility is 33 $cm^2\ V^{-1}\ s^{-1}$ with a diffusion length estimated to be at least 3 μm. The high quality film obtained from the vapour deposited material, having very low trap densities, was assumed to be the origin of the increased mobility. The rate of geminate recombination for solution processed film is lower than the vapour deposited sample, supporting this assertion.[21] This observation is consistent with the THz photoconductivity spectra obtained. As shown in Fig. 5 both the real and imaginary parts of the photoconductivity are positive, a signature of long range charge transport, where the charges do not meet a scattering center within their lifetime. Therefore, the quality of the vapour-deposited film is quite high with less defects and traps.

The results presented so far are obtained from TRTS measurements with a set-up similar to that shown in Fig. 1. A pump probe delay time is varied in order to obtain the photoconductivity kinetics while the gating delay time is fixed at the peak of the THz electric field. In this case, the photoconductivity obtained only represents the lower limit of the mobility. Another approach is to scan the full THz electric field pulse at each of the chosen time delays. Each of the obtained THz electric field responses is then fitted with a Drude or Drude–Smith model to elucidate the charge generation efficiency (quantum yield) and mobility independently.[18] The group of La-o-vorakiat *et al.* implemented such a scheme and the resulting photoconductivity kinetics trace, after fitting with a Drude–Smith model, is shown in Fig. 6.[22] At the earliest timescale, the mobility extracted is about 250 $cm^2\ V^{-1}\ s^{-1}$ and stays constant for about 1 ns. This is the highest reported mobility for a perovskite sample prepared using solution processing.

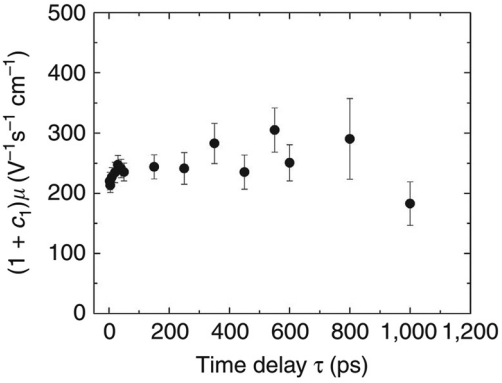

Fig. 6 THz mobility of $MAPbI_3$ obtained from Drude–Smith fits as a function of pump–probe time delay. Reprinted with permission from ref. 22. Copyright (2015) Nature Publishing Group.

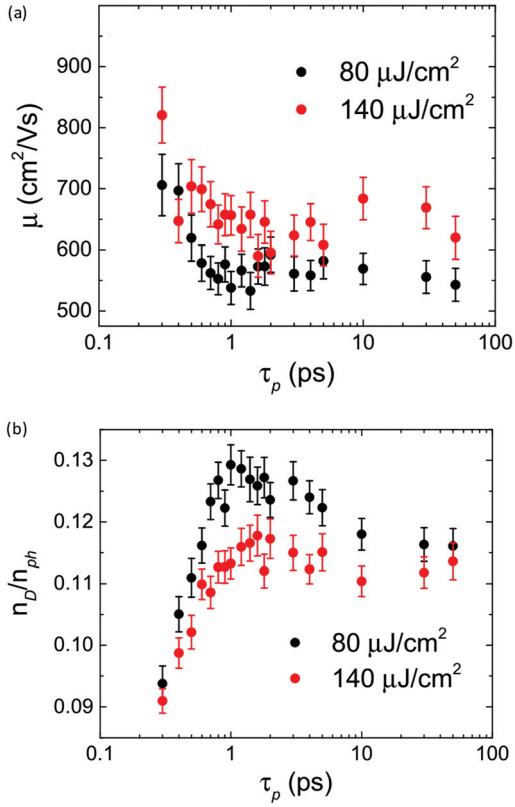

Fig. 7 (a) THz mobility of single crystal $MAPbI_3$ obtained from Drude–Smith fits as a function of pump–probe time delay and (b) concentration of mobile charge carrier per photon absorbed. Reprint with permission from ref. 23. Copyright (2015) Royal Society of Chemistry.

However, the shape of the THz photoconductivity spectrum nevertheless indicates confined charge carrier transport, which is expected for a solution processed sample. Equally interesting, though, is the estimate of the quantum yield (ξ), which is the number of free carriers generated per incident photon absorbed. It was reported in Table 1 of ref. 22 that this value is only 5%. In the work of Ponseca *et al.*[5] and Wehrenfennig *et al.*[20] ξ is assumed to be 1, leading to THz mobility of 20 $cm^2\ V^{-1}\ s^{-1}$ and 11 $cm^2\ V^{-1}\ s^{-1}$ respectively. An equally high mobility (~200 $cm^2\ V^{-1}\ s^{-1}$) as in ref. 22 would, however, be obtained from the measured photo conductivities in ref. 5 and 20, if the same low charge generation yield reported in ref. 22 (ξ = 5%) would be used. This shows that establishing the charge generation yield is essential for correct determination of carrier mobility. In addition, it is important to realize that differences in sample characteristics will lead to more or less subtle differences in the mobilities obtained. Taking these considerations into account, the conclusion indeed is that mobilities are high in these materials.

One of the most attractive characteristics of perovskite solar cell materials is that it can be prepared using kitchen chemistry, that is, by using standard solution processing techniques one can obtain decent power conversion efficiency, *i.e.* >10%. The mobilities presented above are from this solution processed materials deposited to a substrate by spin coating. As such, slight deviations to preparation method would entail different concentration of defects and/or traps and thereby changing and lowering the obtained mobility. In addition, there is also a distribution of crystallographic structures obtained, since solution processing does not have control over details of growth conditions. Therefore, it is of fundamental importance to know the intrinsic material properties, which could represent the upper limit of the performance of perovskite solar cells. In this regard, a single crystalline grown perovskite is of utmost significance in answering these questions.

Valverde-Chávez and co-workers have very recently measured the mobility of single crystal $MAPbI_3$ using TRTS.[23] The approach is similar to that of La-o-vorakiat *et al.*; the full THz electric field response, within a certain frequency range, is obtained at each desired pump probe delay and fits the spectra to a Drude or Drude–Smith model.[23] Unlike in thin films, phonon modes in single crystals are stronger due to continuity of the crystal domain. This presents a complication in measuring single crystal perovskite using the conventional TRTS since the observed modes fall within the THz frequency spectrum of 0.1–2.5 THz.

To circumvent this difficulty, an ultra-broad-band THz pulse is used with a frequency span of 1–30 THz (4–80 meV). Details of generation and detection of this THz pulse, as well as the experimental set-up can be found elsewhere.[24] Fig. 7(a) shows the time dependence of mobility obtained from global fits of a Drude model to the experimental spectra taken at two fluences. The rise of the THz photoconductivity kinetics is about 40 fs, while the shape of the kinetic traces clearly show long range transport. At the earliest timescale, the mobility is about 800 $cm^2\ V^{-1}\ s^{-1}$ and then relaxes to about 550 $cm^2\ V^{-1}\ s^{-1}$ after about 100 ps for both fluences. Such very high mobility can be directly correlated to the almost perfect crystallinity of the single crystal, as well as the very small density of defects. However, a noticeable rise in the mobile carrier charge generation efficiency (quantum yield) is observed on the sub-

ps timescale, *i.e.* from 9% to about 13%, which could also explain the decrease of mobility, Fig. 7(b). Thus, examining the shape of the THz spectra, it was concluded that this is due to dynamic screening of infrared active phonons and background Debye relaxation of the CH_3NH^{+3} cation brought about by the photogenerated free charge population. The mobility measured here could probably represent the upper limit of the intrinsic mobility of this material. We note however that there are also several ways to grow single crystal perovskites. One can expect that each of these methods could lead to a lesser concentration of defects and therefore higher mobility.

There are also efforts in understanding the temperature dependence of these materials using TRTS. In the work of Milot *et al.*, an increase in the mobility of charge carriers (~150 $cm^2\ V^{-1}\ s^{-1}$) were probed as the temperature is lowered (77 K, orthorhombic phase).[25] They found that there is a $t^{-1.5}$ dependence in the mobility, very similar to that of silicon.[26] Similar results were obtained by the group of Karakus *et al.*, (~150 $cm^2\ V^{-1}\ s^{-1}$ at 77 K) which they surmised as due to less phonon–electron interaction at low temperature.[27] In the later timescale, *i.e.* from hundreds of ns to few us, we obtained analogous temperature dependence which were assigned to quieting of phonons.[12]

3. Charge transfer to organic acceptor materials

The use of organic acceptor materials could be more compatible with the OMHP than metal oxides, since these molecules are also prepared by solution processing similar to the active perovskite material. The most commonly used are PCBM as electron transporting molecule and Spiro-OMeTAD for hole transfer. The dynamics of charge transfer from $MAPbI_3$ to these molecules are not so well studied and this section of the mini-review presents the timescale of injection from the perovskite to the organic charge acceptor using TRTS.

The photoconductivity kinetics of neat $MAPbI_3$, as well as $MAPbI_3$/PCBM and $MAPbI_3$/Spiro-OMeTAD are shown in Fig. 8. The TRTS mobility measured for this particular sample of neat perovskite is the highest (15 $cm^2\ V^{-1}\ s^{-1}$) and there is a relatively small decay up to 1 ns. The $MAPbI_3$/Spiro-OMeTAD photoconductivity kinetics are similar, but its mobility, already at the earliest times, is at least three times lower, *i.e.* 5 $cm^2\ V^{-1}\ s^{-1}$. This means that either charges have recombined on a time scale shorter than the instrument response of the set-up, or the reduction of the signal is due to disappearance of holes or electrons. From previous studies it is known that charge recombination occurs on many ns to μs time scale, strongly dependent on carrier density.[5,14] Therefore, this mechanism can be ruled out as explanation of the reduced signal. Consequently, this suggests that the observed differences in mobility of the two samples is due to a very fast injection of holes from the perovskite to Spiro-OMeTAD. The large energy offset between the valence bands of $MAPbI_3$ and Spiro-OMeTAD

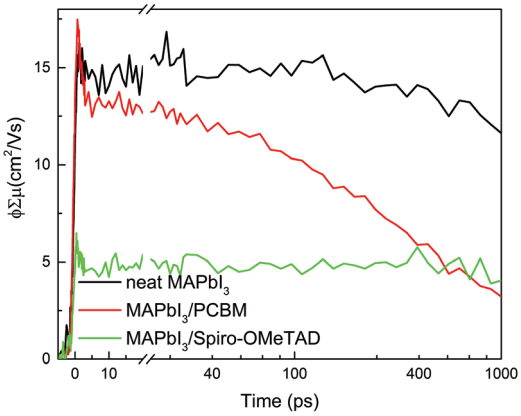

Fig. 8 TRTS photoconductivity kinetics of neat $MAPbI_3$, $MAPbI_3$/PCBM and $MAPbI_3$/Spiro-OMeTAD for 1 ns. Reprint with permission from ref. 30. Copyright 2015 American Chemical Society.

(0.57 eV),[28] is enough to promote sub-ps hole injection, despite the fact that no additives, *e.g.* LiTFSI, or similar was added in this sample. A recent optical transient absorption study of hole injection found that charge transfer from the perovskite to Spiro-OMeTAD is 0.7 ps.[29] The mobility measured for $MAPbI_3$/Spiro-OMeTAD, which is 5 $cm^2\ V^{-1}\ s^{-1}$ should therefore be due to the electrons left in the conduction band of the perovskite, since holes are already in the Spiro-OMeTAD. For at least 1 ns, these electrons remain mobile and could not find any traps and/or holes to recombine with as the photoconductivity kinetics remain flat up to this time scale. The mobility measured in this sample is somewhat lower than that reported in the previous section. This can be explained, as mentioned several times before, by different preparation conditions during sample growth. Moreover, we concluded that in these particular samples, the perovskite is an unintentionally p-doped material that could have removed the photoinduced electrons even before the probe pulse arrived. Detailed discussion of this can be found elsewhere.[30]

The initial THz mobility of the $MAPbI_3$/PCBM sample is 15 $cm^2\ V^{-1}\ s^{-1}$ very similar to that of neat $MAPbI_3$. However, a slow decay is noticeable after a few hundred ps and the total signal is reduced to about a third after 1 ns. This means that at the earliest time scale, both electrons and holes are generated in the perovskite but then slowly disappearing. As explained above, such decay could be either recombination or injection. From literature it is known that PCBM has been used as electron accepting and transporting material[31,32] and therefore it can be surmised that this decay, at least partially, reflects electron injection from $MAPbI_3$ to PCBM.[33] Moreover, the small offset between the conduction bands of perovskite and PCBM (0.3 eV), could retard the injection process.[28] Electron injection from perovskite to PCBM as reported by Xing *et al.* using transient absorption spectroscopy (0.4 ns) falls within the timescale of photoconductivity decay observed here (Fig. 7). If one on the other hand assumes that electron injec-

tion is faster than a few tens of ps, then the initial THz photoconductivity kinetics should have been lower than that seen in neat $MAPbI_3$ since electrons would have already disappeared, which is not the case here. Once injected into PCBM, electrons will be pinned very close to the interface, because of the low electron mobility in PCBM ($\sim 10^{-3}$ cm^2 V^{-1} s^{-1}).[6] This inevitably leads to electron recombination with the photoexcited holes in the valence band of perovskite and probably also with the dark holes present as a result of the unintentional p-doping.[33] Excitation dependent second order recombination could occur on the same timescale as well. However, looking at the flat kinetics of the neat perovskite, one can disregard this process. Finally, it can be concluded that the hundreds of ps decay in the $MAPbI_3$/PCBM photoconductivity kinetics is a result of a convolution of two processes – electron injection and recombination between injected electrons in PCBM and holes in the perovskite.[33]

4. Summary and outlook

Measurements of mobility in thin films of $MAPbI_3$ perovskite yielded similar results from different groups. Subtle differences observed are probably to a large extent related to differences in the methods employed in sample preparation. Higher mobility is obtained for a single crystal perovskite, which is due to lower concentration of defects. Mechanism of charge injection is shown to be influenced by the energy band alignment between the perovskite and organic electrodes, while its recombination is strongly influenced by unintentional p-doping of the perovskite, an effect brought about by the concentration of defects that traps electrons. All of these results point to a very important parameter that controls charge carrier dynamics in these materials: defects. The state and concentration of defects, brought about by different preparation routes and protocols, should be foremost concern in order to realize a better performing solar cell.

Through the use of time resolved THz spectroscopy, these early time processes in perovskite solar cell materials were obtained. There are two other possible ways where TRTS can contribute in understanding the charge carrier dynamics in these materials. First is to investigate the photophysics of perovskite in nanometer scale, that is, by focusing the THz pulse into the tip of an scanning tunnelling microscope (STM) similar to that demonstrated by Cocker *et al.* in gold nanoislands.[34] Using this scheme, investigations of defect sites could be possible since a 2 nm spatial resolution was obtained in that work. Another approach is to use TRTS in scanning large scale, commercial-size, *e.g.* in the order of 1 m^2, perovskite solar panel. This could help in mapping defect zones within the panel and identify possible faults in manufacturing commercial scale solar cells. Both in these micro- and macrometer strategies, TRTS can be proven valuable not only in revealing fundamental processes but also in providing insights for possible optimization of processes for solar cell industry.

Acknowledgements

This work was supported by the Swedish Energy Agency (STEM), the Swedish Research Council, the Knut&Alice Wallenberg foundation, the European Research Council (Advanced Investigator Grant to VS, 226136-VISCHEM), the nanometer Consortium at Lund University (nmc@LU) and the Lund Laser Center.

Notes and references

1 Anon National Renewable Energy Laboratory efficiency chart (2015); http://www.nrel.gov/ncpv/images/efficiency_chart.jpg, *Natl. Renew. Energy Labs Effic. chart*, 2015.
2 H. Zhu, Y. Fu, F. Meng, X. Wu, Z. Gong, Q. Ding, M. V. Gustafsson, M. T. Trinh, S. Jin and X.-Y. Zhu, *Nat. Mater.*, 2015, **14**, 636–642.
3 J. Luo, J.-H. Im, M. T. Mayer, M. Schreier, M. K. Nazeeruddin, N.-G. Park, S. D. Tilley, H. J. Fan and M. Grätzel, *Sci.*, 2014, **345**, 1593–1596.
4 J. B. Baxter and C. a. Schmuttenmaer, *J. Phys. Chem. B*, 2006, **110**, 25229–25239.
5 C. S. Ponseca, T. J. Savenije, M. Abdellah, K. Zheng, A. Yartsev, T. Pascher, T. Harlang, P. Chabera, T. Pullerits, A. Stepanov, J. P. Wolf and V. Sundström, *J. Am. Chem. Soc.*, 2014, **136**, 5189–5192.
6 C. S. Ponseca, H. Němec, N. Vukmirović, S. Fusco, E. Wang, M. R. Andersson, P. Chabera, A. Yartsev and V. Sundström, *J. Phys. Chem. Lett.*, 2012, **3**, 2442–2446.
7 C. S. Ponseca, A. Yartsev, E. Wang, M. R. Andersson, D. Vithanage and V. Sundström, *J. Am. Chem. Soc.*, 2012, **134**, 11836–11839.
8 N. Vukmirović, C. S. Ponseca, H. Němec, A. Yartsev and V. Sundström, *J. Phys. Chem. C*, 2012, **116**, 19665–19672.
9 H. Němec, J. Rochford, O. Taratula, E. Galoppini, P. Kužel, T. Polívka, A. Yartsev and V. Sundström, *Phys. Rev. Lett.*, 2010, **104**, 197401.
10 K. Žídek, K. Zheng, C. S. Ponseca, M. E. Messing, L. R. Wallenberg, P. Chábera, M. Abdellah, V. Sundström and T. Pullerits, *J. Am. Chem. Soc.*, 2012, **134**, 12110–12117.
11 C. S. Ponseca, H. Němec, J. Wallentin, N. Anttu, J. P. Beech, A. Iqbal, M. Borgström, M. E. Pistol, L. Samuelson and A. Yartsev, *Phys. Rev. B: Condens. Matter*, 2014, **90**, 1–7.
12 T. J. Savenije, C. S. Ponseca, L. Kunneman, M. Abdellah, K. Zheng, Y. Tian, Q. Zhu, S. E. Canton, I. G. Scheblykin, T. Pullerits, A. Yartsev and V. Sundström, *J. Phys. Chem. Lett.*, 2014, **5**, 2189–2194.
13 A. Miyata, A. Mitioglu, P. Plochocka, O. Portugall, J. T.-W. Wang, S. D. Stranks, H. J. Snaith and R. J. Nicholas, *Nat. Phys.*, 2015, **11**, 582–587.
14 Q. Lin, A. Armin, R. Chandra, R. Nagiri, P. L. Burn and P. Meredith, 2014.
15 T. C. Sum and N. Mathews, *Energy Environ. Sci.*, 2014, **7**, 2518–2534.

16 C. Sheng, C. Zhang, Y. Zhai, K. Mielczarek, W. Wang, W. Ma, A. Zakhidov and Z. Valy Vardeny, *Phys. Rev. Lett.*, 2015, **114**, 116601.
17 S. Sun, T. Salim, N. Mathews, M. Duchamp, C. Boothroyd, G. Xing, T. C. Sum and Y. M. Lam, *Energy Environ. Sci.*, 2014, **7**, 399.
18 E. Hendry, M. Koeberg, B. O'Regan and M. Bonn, *Nano Lett.*, 2006, **6**, 755–759.
19 D. K. Ferry and J. P. Bird, *Electronic Materials and Devices*, Academic Press, London, 2001.
20 C. Wehrenfennig, G. E. Eperon, M. B. Johnston, H. J. Snaith and L. M. Herz, *Adv. Mater.*, 2014, **26**, 1584–1589.
21 C. Wehrenfennig, M. Liu, H. J. Snaith, M. B. Johnston and L. M. Herz, *Energy Environ. Sci.*, 2014, **7**, 2269.
22 C. La-o-vorakiat, T. Salim, J. Kadro, M.-T. Khuc, R. Haselsberger, L. Cheng, H. Xia, G. G. Gurzadyan, H. Su, Y. M. Lam, R. a. Marcus, M.-E. Michel-Beyerle and E. E. M. Chia, *Nat. Commun.*, 2015, **6**, 7903.
23 D. A. Valverde-Chávez, C. Ponseca, C. Stoumpos, A. Yartsev, M. G. Kanatzidis, V. Sundström and D. G. Cooke, *Energy Environ. Sci.*, 2015, **8**, 3700–3707.
24 D. G. Cooke, F. C. Krebs and P. U. Jepsen, *Phys. Rev. Lett.*, 2012, **108**, 056603.
25 R. L. Milot, G. E. Eperon, H. J. Snaith, M. B. Johnston and L. Herz, *Adv. Funct. Mater.*, 2015, **25**, 6218–6227.
26 B. van Zeghbroeck, *Principles of Semiconductor Devices*, University of Colorado, Boulder CO, 2006.
27 M. Karakus, S. A. Jensen, F. D'Angelo, D. Turchinovich, M. Bonn and E. Canovas, *J. Phys. Chem. Lett.*, 2015, **6**, 4991–4996.
28 G. Xing, N. Mathews, S. Sun, S. S. Lim, Y. M. Lam, M. Grätzel, S. Mhaisalkar and T. C. Sum, *Science*, 2013, **342**, 344–347.
29 P. Piatkowski, B. Cohen, J. F. Ramos, M. R. Di Nunzio, N. Mohammad, K. M. Grätzel, S. Ahmad and A. Douhal, *Phys. Chem. Chem. Phys.*, 2015, **17**, 14674–14684.
30 E. M. Hutter, G. E. Eperon, S. D. Stranks and T. J. Savenije, *J. Phys. Chem. Lett.*, 2015, **6**, 3082–3090.
31 Q. Shen, Y. Ogomi, J. Chang, S. Tsukamoto, K. Kukihara, T. Oshima, N. Osada, K. Yoshino, K. Katayama, T. Toyoda and S. Hayase, *Phys. Chem. Chem. Phys.*, 2014, **16**, 19984.
32 O. Malinkiewicz, A. Yella, Y. H. Lee, G. M. M. Espallargas, M. Graetzel, M. K. Nazeeruddin and H. J. Bolink, *Nat. Photonics*, 2014, **8**, 128–132.
33 C. S. Ponseca, Jr., E. M. Hutter, P. Piatkowski, B. Cohen, T. Pascher, A. Douhal, A. Yartsev and V. Sundström, *J. Am. Chem. Soc.*, 2015, **137**, 16043–16048.
34 T. L. Cocker, V. Jelic, M. Gupta, S. J. Molesky, J. A. J. Burgess, G. De Los Reyes, L. V. Titova, Y. Y. Tsui, M. R. Freeman and F. A. Hegmann, *Nat. Photonics*, 2013, **7**, 620–625.